

Deep Learning Models for SO₂ Distribution in a 30 MW Boiler via Computational Fluid Dynamics Simulation Data

Zhenhao Tang,* Hongrui Dong, Chong Zhang, Shengxian Cao, and Tinghui Ouyang

Cite This: *ACS Omega* 2022, 7, 41943–41955

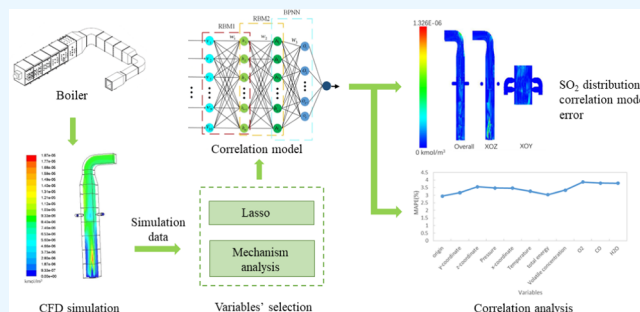
Read Online

ACCESS |

Metrics & More

Article Recommendations

ABSTRACT: The distribution of SO₂ in a boiler is an important factor affecting tube corrosion in a furnace. To investigate the correlation between SO₂ distribution and numerous variables (e.g., temperature, O₂ distribution, etc.), a hybrid deep learning model is developed via the computational fluid dynamics (CFD) simulation data. First, the combustion process under typical working conditions is simulated to output the training data set. Then, a LASSO algorithm is adopted to select input variables with a high correlation with SO₂ distribution. Finally, a deep belief network combined with a restricted belief machine and a fully connected layer is developed to describe the nonlinear relationship. The proposed model is the first work to use a deep learning algorithm to obtain the correlation between SO₂ distribution and other products of combustion. The results show that O₂ concentration has the highest influence on SO₂ distribution.



1. INTRODUCTION

The combustion process in coal-fired boilers includes complex physical and chemical reactions in the furnace. In this process, excessive SO₂ is generated, which will damage the internal structure of the boiler.^{1–3} Therefore, it is necessary to study the influence of the products of combustion (POCs) in the furnace on SO₂ distribution and provide theoretical support for the subsequent control and emission reduction of SO₂ and other gases. However, the distribution of SO₂ in the furnace is affected by the pulverized coal composition, air distribution mode, different operating conditions, boiler structure, and many other factors.⁴ This makes the study of SO₂ distribution a difficult problem in the current research.

Computational fluid dynamics (CFD) technology is widely used to analyze and simulate the distribution of POCs, such as temperature field,^{5–8} O₂ distribution,⁹ NO_x emission,^{10,11} and NO_x distribution,¹² in the combustion boiler. The accuracy of the simulations of CFD technology had been validated.^{13,14} Du et al.¹³ performed numerical validation on a 500 MW wall-fired boiler, and Tan et al.¹⁴ developed and validated a numerical model to study the effect of burner tilt angle on the temperature and species distribution of a 700 MW pulverized coal-fired boiler with deep space staging technology. Therefore, it is feasible to select CFD simulation data to analyze SO₂ distribution.

With the development of computing technology, machine learning methods including artificial neural network (ANN),¹⁵ support vector regression (SVR),¹⁶ extreme learning machine (ELM),¹⁷ and Kriging¹⁸ have been applied in various fields. Also, these methods were successfully applied to construct the

relationship between boiler emission products and operating parameters, involving boiler temperature prediction,¹⁹ NO_x emission prediction,^{20–23} and SO₂ emission prediction.^{24–29} Krzywanski et al.^{24,25} established a SO₂ emission prediction model for a coal-fired boiler based on ANN; Wen et al.²⁶ established a SO₂ emission model based on a 12/6/1 three-layered back-propagation neural network (BPNN); Yu et al.²⁷ took an ELM as the main model to predict SO₂ emissions from a CFB boiler; Peng et al.²⁸ adopted fuzzy association rule mining to establish a SO₂ emission model; and Pai et al.²⁹ used the gray model (GM) to predict CO₂, SO₂, and O₂ in the emissions. The above studies have effectively mined the relationships between data and used data-driven algorithms to establish a SO₂ emission prediction model. From the literature survey, the research on SO₂ by machine learning methods mainly focuses on emission prediction, but there is little research on the correlation between SO₂ and other POC. It is very necessary for accurate control of the combustion process to improve the corrosion of the internal tube wall of the boiler, which is the authors' motivation.

The deep belief network (DBN) is a deep learning algorithm consisting of a restricted Boltzmann machine (RBM) and

Received: June 3, 2022

Accepted: October 27, 2022

Published: November 11, 2022



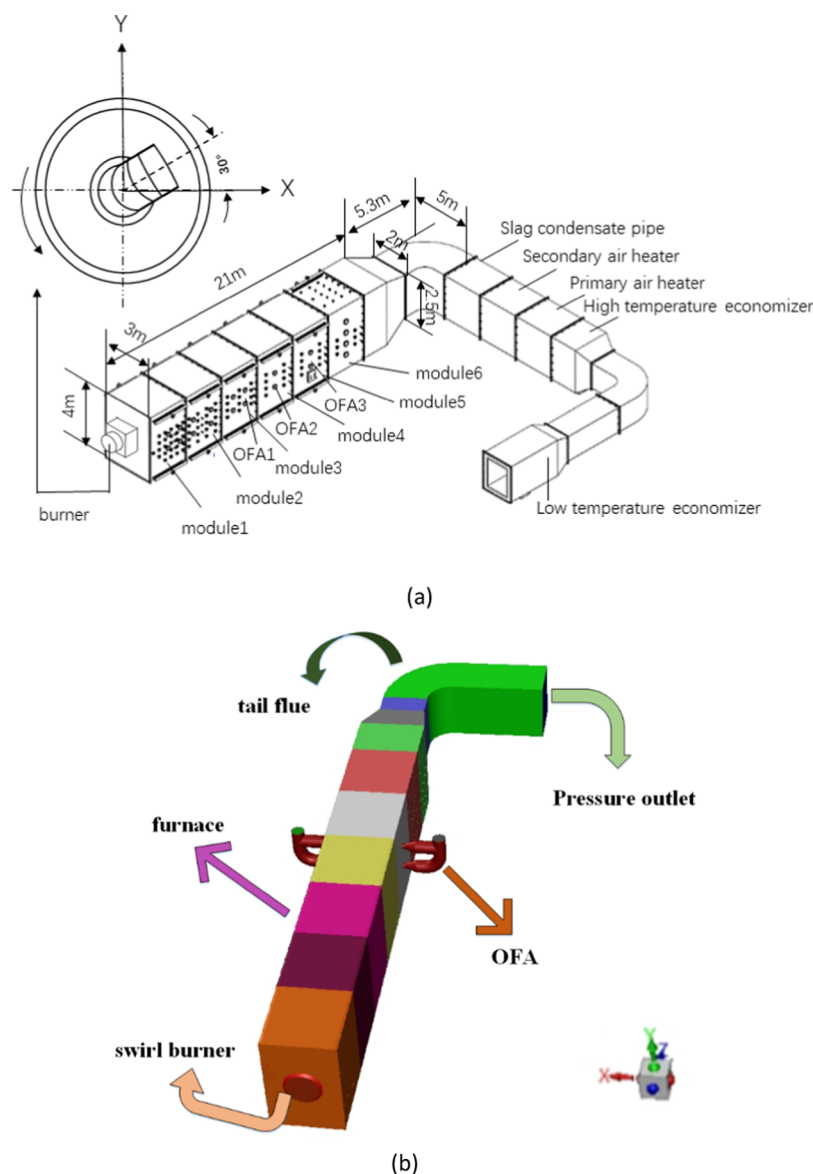


Figure 1. 30 MW test furnace: (a), (b) its schematic diagram and physical model.

BPNN. Since DBN was proposed by Hinton et al.,³⁰ it has been widely used in the fields of pattern recognition, image classification, and fault diagnosis.^{31,32} DBN used in the multiobjective optimization for combustion system operations offered a more accurate and robust performance.²² The least absolute shrinkage and selection operator (LASSO) algorithm³³ can select the feature variables with high correlation and remove some redundant variables from numerous variables, not only decreasing the training time but also improving the quality of the model. Therefore, in this paper, a novel deep learning model, i.e., a numerical simulation data-based LASSO-DBN algorithm, is proposed for the first time to analyze the correlation between the SO_2 distribution of a 30 MW boiler and other POCs.

The contributions of this work are as follows:

- (1) The correlation between boiler SO_2 concentration distribution and other POCs was studied. Since it is difficult to obtain all of the SO_2 at each point inside the furnace, the CFD numerical simulation data is used as the experimental data of the model, which provides the data basis for establishing the model.

- (2) The LDBN model was established based on the feature selection method of removing redundant features and the deep learning model, and it revealed the relationship between SO_2 distribution, temperature, O_2 , CO, and many other variables.

The rest of this paper is as follows. In Section 2, to obtain numerical simulation data of SO_2 distribution, a CFD model for a 30 MW furnace is established according to the geometry and physical parameters of the furnace and then SO_2 distribution is simulated under typical working conditions by the CFD model using ANSYS Fluent commercial software. Section 3 presents the modeling process to predict SO_2 distribution and a LASSO algorithm to determine the selected variables from numerous variables of the normalized raw data obtained in Section 2 and develops a DBN model to construct SO_2 distribution with high correlation variables in real time. Section 4 analyzes and discusses related experimental results, including sensitivity analysis of variables of SO_2 distribution and comparison of the proposed deep learning model with three other models to

validate the effectiveness and accuracy. Section 5 draws conclusions.

2. CFD SIMULATIONS OF SO₂ DISTRIBUTION IN THE FURNACE UNDER TYPICAL OPERATING CONDITIONS

The research object of this study is a 30 MW furnace of a coal-fired boiler. To establish a deep learning model of SO₂ distribution in the furnace, the driving data of the model needs to be determined first. To this end, the CFD model of the furnace is established and CFD simulations under typical operating conditions are conducted by ANSYS FLUENT in this section.

2.1. Description of the 30 MW Furnace. The 30 MW furnace is equipped with a single 1:1 swirl burner, as shown in Figure 1a. The furnace has a hearth section of 3 m × 4 m and a combustion zone length of 21 m. The whole test bench adopts a modular assembly structure, which is mainly composed of six modules. The internal top and bottom sides of the furnace are arranged with water-wall tubes to absorb the radiation heat from the high-temperature combustion products in the furnace chamber. The adiabatic insulation structure is formed on the left and right sides to facilitate the simulation of the actual boiler flue gas flow field temperature. The furnace is horizontally arranged in a U shape, and three groups of overfire air burners are respectively arranged on both sides of the hearth at 8, 10.5, and 13.5 m away from the burner nozzle for combustion adjustment.

According to the configuration and the size of the furnace, and to facilitate the simulation of the furnace by CFD, it is assumed that only the combustion area and the tail flue area are considered, and the burnt-out windpipe 13.5 m away from the burner nozzle is reserved for regulating combustion. Thus, the furnace is simplified for the establishment of the physical model, as shown in Figure 1b. The entire physical model has a length of 3 m, a width of 4 m, and a height of 26.3 m. The tail flue is 5 m in length, and the coordinate origin is set at the geometric center point of the bottom. A single swirl burner is arranged at the bottom. The load for numerical simulations is 30 MW. The design angles of the swirl burner blades are from 0 to 60°. In this numerical simulation, six burner blade angles, i.e., 10, 20, 30, 45, 55, and 65°, are designed. The air distribution method of the burner is as follows: the primary air is mixed with pulverized coal, the primary air and the secondary air enter the furnace, respectively, and then the tertiary air and central air are omitted. The main simulation process of pulverized coal concentration in the furnace includes the determination of main parameters, the establishment of a combustion model, analysis of numerical simulation results, etc. According to the basic conservation equation and the physical structure of the actual combustion test bench,³⁴ the following assumptions are made:

- (1) The working fluid of flue gas in the furnace is an incompressible ideal gas.
- (2) All temperature distributions and changes are uniformly changed.
- (3) The water wall and other media are regarded as ash.
- (4) Convective heat transfer is not considered, and only radiation heat transfer is considered.
- (5) There is no heat dissipation and air leakage inside.

2.2. CFD Modeling of the Furnace. The mesh division is mainly conducted by preprocessing software GAMBIT of Fluent. The calculation area adopts the hybrid grid, which can

adapt to various complex geometric models and has a good local encryption function. The main areas of the furnace including the burner area, the upper part of the burner, and the tail flue area are all structured mesh. The main combustion reaction occurs in the interval of 0–15 m, which is of high importance. The analysis of the combustion results should focus on this area. Therefore, the grid in this interval needs to be refined. However, the physical structure of the overfire air tube is complex, and there is no need to pay attention to the internal combustion situation, so the unstructured grid drawing method is adopted for the overfire air tube on both sides. The number of grids after division is 1.2 million. The sectional views of the mesh section are shown in Figure 2.

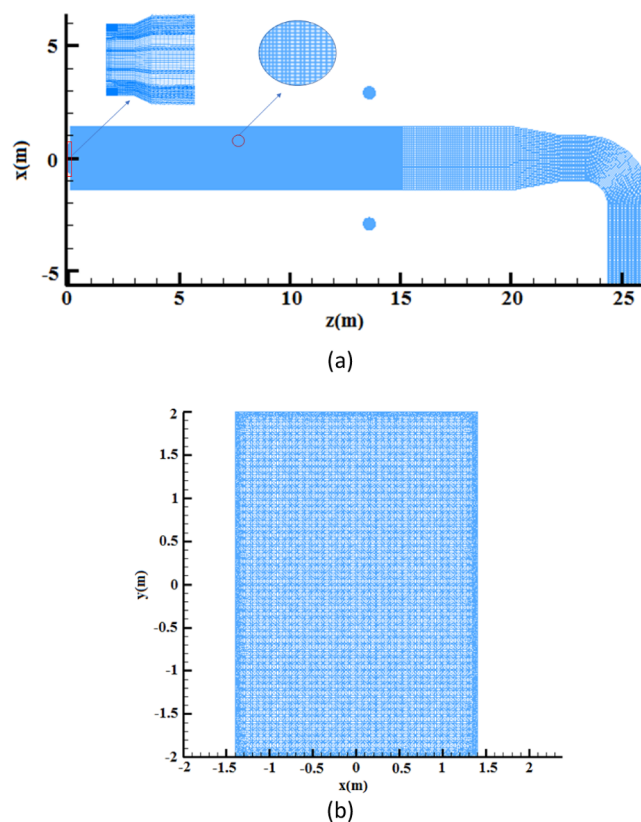


Figure 2. Burner cross-sectional grid: (a) grid in the x – z direction and (b) grid in the x – y direction.

According to the analysis of the actual operation of the furnace, the realizable k – ϵ model, stochastic particle orbit model, single-rate equation model, species transport model, kinetics/diffusion model, and DO model are selected by ANSYS Fluent software for numerical simulations, and the boundary conditions are set as shown in Table 1.

2.3. CFD Analysis of the Furnace. The oxygen content and outlet velocity are selected as the convergence judgment conditions. Meanwhile, simulation calculations are conducted for the operating conditions of burner swing angles of 10, 20, 30, 45, 55, and 65°. The results of the temperature distribution, SO₂ concentration distribution, O₂ concentration distribution, and other data in the furnace during steady-state operation of the boiler are obtained. Then, the simulation results are output by the export function of ANSYS Fluent software. The results of the simulation of SO₂ distribution of the angle to 30° condition and 55° condition are shown in Figure 3.

Table 1. Description of Boundary Conditions

serial number	name of the variables	unit	values
1	moisture (received basis)	%	20.00
2	ash (received basis)	%	10.00
3	calorific value (received basis)	kJ/kg	20 933
4	volatile (received basis)	%	39.56
5	average excess air coefficient		1.20
6	carbon (received basis)	%	55.10
7	hydrogen (received basis)	%	3.50
8	oxygen (received basis)	%	9.60
9	nitrogen (received basis)	%	0.80
10	sulfur (received basis)	%	1.00
11	the total amount of coal	t/h	5.196
12	total air flow	t/h	86.123
13	primary air flow	t/h	14.745
14	secondary air flow	t/h	44.234
15	overfire air flow	t/h	27.144
16	primary air temperature	°C	300
17	secondary air temperature	°C	350
18	environment temperature	°C	30

The CFD simulation results under the typical operating conditions provide raw data onto the deep learning model for correlation analysis of SO₂ distribution in the furnace.

3. LASSO-DBN MODEL OF SO₂ DISTRIBUTION IN THE FURNACE

The establishment of the correlation analysis model of SO₂ distribution in the furnace mainly consists of three parts: data preprocessing, variable selection, and LDBN algorithm modeling. The whole process of modeling is shown in Section 3.1. The min–max method is used for data normalization in data preprocessing, and it is described in Section 3.2. The selection of variables is divided into two parts: mechanism analysis and feature selection, and the specific method is shown in Section 3.3. Finally, as shown in Section 3.4, the correlation analysis between the SO₂ concentration distribution and other POCs is realized using the DBN algorithm.

3.1. Description of LDBN Modeling. The process of establishing the SO₂ distribution correlation analysis model is shown in Figure 4.

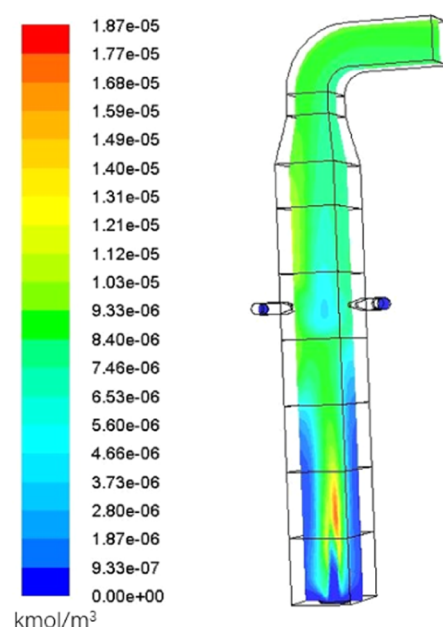
Step 1: Select the data output by CFD simulations as the modeling data.

Step 2: Preprocess the simulation data to build a reliable data set.

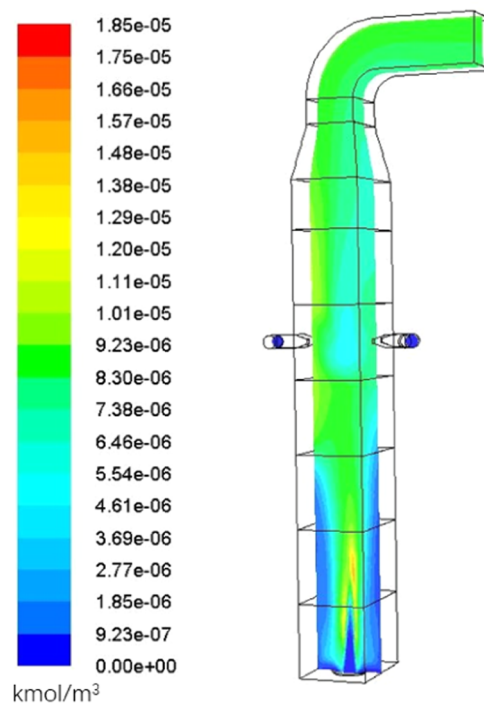
Step 3: Select relevant variables according to experience and mechanism analysis and use the Lasso method to select variables and remove some redundant variables.

Step 4: Select highly correlated variables as the modeling input and establish a DBN-based correlation model of SO₂ distribution in the furnace. Compare the established model with other algorithm models to verify the accuracy and stability of the model.

3.2. Normalization. The simulation data have different dimensions and orders of magnitude. If the original data is directly used as the input data for model training, only the influence of the data with a higher numerical value will be highlighted in the modeling process, and the data with a lower numerical level will be ignored. Therefore, to eliminate the difference in dimensionality, the min–max method is used to normalize the simulation data. The normalization is defined as follows



(a)



(b)

Figure 3. Result of CFD analysis of SO₂ distribution of the angle: (a) 30° condition and (b) 55° condition.

$$y_i^* = \frac{y_i - y_{\min}}{y_{\max} - y_{\min}} \quad (1)$$

where y_i is the original value, y_i^* is the normalized value, and y_{\min} and y_{\max} are the minimum and maximum values, respectively.

3.3. Variables' Selection. **3.3.1. Mechanistic Analysis.** According to the combustion mechanism, the thermal stability of different sulfur components in the fuel in the furnace is different. The sulfur element in the fuel is mainly separated out

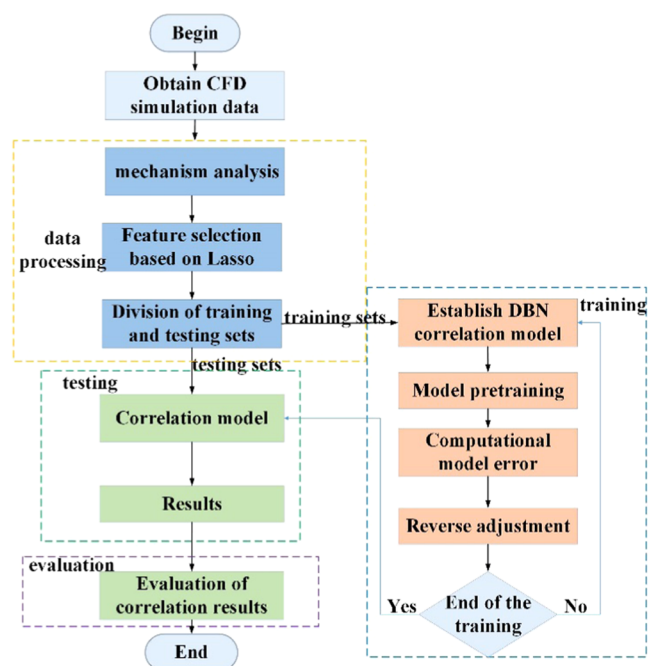
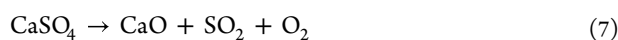
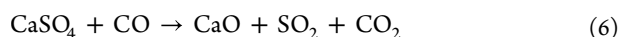
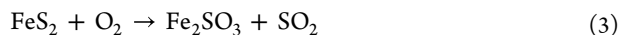


Figure 4. Framework of the SO₂ distribution correlation model based on LDBN.

as H₂S and COS. Combustible sulfur reacts with O₂ to generate SO₂, while noncombustible sulfur is easy to decompose at high temperatures to generate SO₂.³⁵ The chemical equations are shown as follows



It can be seen from the above combustion mechanisms that the formation of SO₂ in the furnace is related to the temperature, total energy, O₂ concentration, CO concentration, and other POC concentrations. Therefore, 23 relevant variables are selected from the simulation data based on experience and mechanism analysis.

3.3.2. Feature Selection. Because the simulation data has the characteristics of uneven quality, high dimension, and little correlation, it will not only increase the training time but also reduce the quality of the model. Thus, it is necessary to select the features of this data.

Tibshirani³³ proposed the Lasso algorithm, which can select the variables with high correlation and remove some redundant variables that do not affect or even reduce the accuracy of the model. In this study, the Lasso method is adopted to screen out ten variables highly correlated with SO₂ concentration by formulas 8 and 9 from 23 variables such as temperature, energy, x-velocity, y-velocity, and z-velocity.

$$\arg \min_{\beta} \left\{ \sum_{i=1}^n \left(y_i - \beta_0 - \sum_{j=1}^p x_{ij} \beta_j \right)^2 \right\} \quad (8)$$

$$\text{subject to } \sum_{j=1}^p |\beta_j| \leq s \quad (9)$$

where β_j is the regression coefficient of the j th variable; $s \geq 0$ is the adjustment parameter, and it is a normal punishment for the regression coefficient.

According to the screening results, 13 variables are removed, and the remaining 10 variables, such as O₂ concentration and temperature, are highly correlated with SO₂ concentration.

3.4. DBN Algorithm of SO₂ Distribution. The DBN model consists of a restricted Boltzmann machine (RBM) and a back-propagation neural network (BPNN). A single RBM is composed of a visible layer (v) and a hidden layer (h). The neurons in the same layer are not connected and do not affect each other, while the neurons in different layers are connected unidirectionally. The structure of the SO₂ distribution correlation analysis model based on DBN is shown in Figure 5. First, the parameters of the whole DBN model are initialized

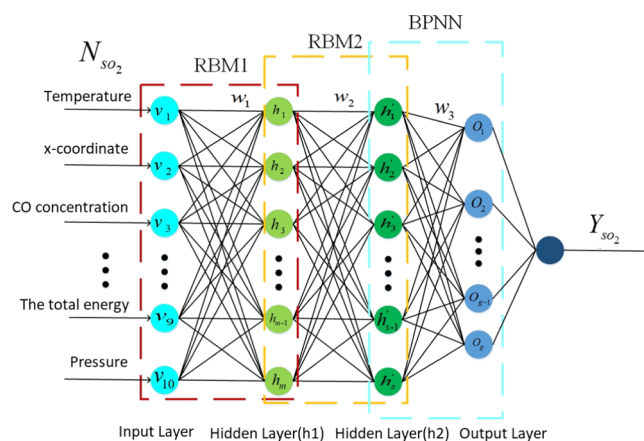


Figure 5. DBN model for SO₂ distribution correlation analysis.

layer by layer by using the left-to-right unsupervised learning method. Then, the right-to-left supervised learning method is used to fine-tune the network parameters.

In the process of unsupervised learning, the simulation data is input through the bottom layer of DBN, and the parameters of the RBM network are initialized randomly. Meanwhile, the number of layer nodes and the maximum number of layers of the DBN network are set. The output of low-level RBM is used as the input of high-level RBM. Each RBM is fully trained, and the network parameters are continuously updated. In the fine-tuning stage, the BPNN of the last layer is trained. The errors are propagated back layer by layer, and the overall weight is fine-tuned and optimized. Finally, a correlation analysis model between SO₂ concentration distribution and other POCs is established.

The correlation analysis model of SO₂ in the furnace based on DBN can be written as follows

$$Y_{\text{so}_2} = f(N_{\text{so}_2}, w_1, w_2, w_3, b) \quad (10)$$

where Y_{so_2} is the s th value of SO₂ concentration; N_{so_2} is an input variable for SO₂ concentration; w_1 , w_2 , and w_3 represent the weights of different layers in the SO₂ distribution correlation analysis model based on DBN; and b is the bias.

4. RESULTS AND DISCUSSION

In this study, the combustion state can be changed by changing the swing angle of the burner while the working conditions such as boiler load, coal type, and air flow are fixed. Therefore, this design can establish the overall distribution of SO₂ in the furnace under different burner blade swing angles.

To verify the validity of the model established in this paper, the correlation analysis of SO₂ concentration under different working conditions is performed. Since there are about 1.2 million three-dimensional coordinate points in the boiler furnace, it takes a long time to build a distributed model using all the data. Therefore, the furnace is partitioned according to the standard of *x*-coordinate in ascending order, and the simulation data is divided into eight data sets. For the convenience of subsequent description, the data sets are denoted Data 1, Data 2, Data 3, Data 4, Data 5, Data 6, Data 7, and Data 8.

In Section 2, the origin of coordinates is set at the bottom center, but there is a tail flue area in the furnace, and the *x*-coordinate range is [−6.03, 3.19]. The modeling data division is shown in Table 2. The Lasso method is used to select the

Table 2. Data Division

data set	<i>x</i> -coordinate range	number of training set data	number of test set data
Data 1	[−6.03 × 10 ⁰ , −1.26 × 10 ⁰]	662 409	134 371
Data 2	[−1.25 × 10 ⁰ , −8.21 × 10 ^{−1}]	746 977	151 625
Data 3	[−8.20 × 10 ^{−1} , −4.46 × 10 ^{−1}]	741 846	148 847
Data 4	[−4.45 × 10 ^{−1} , −4.16 × 10 ^{−2}]	755 877	150 057
Data 5	[−4.15 × 10 ^{−2} , 3.16 × 10 ^{−1}]	762 412	151 459
Data 6	[3.62 × 10 ^{−1} , 7.59 × 10 ^{−1}]	764 341	152 389
Data 7	[7.60 × 10 ^{−1} , 1.13 × 10 ⁰]	659 177	131 446
Data 8	[1.14 × 10 ⁰ , 3.19 × 10 ⁰]	653 746	131 076

features of the eight data sets. From 23 variables such as energy, temperature, coordinates, and furnace product concentration, 10 variables with high correlation are selected as the input of the DBN model, and SO₂ concentration in the furnace is used as the output variable for the model. The sort order for the importance of the variables and modeling data information is shown in Tables 3 and 4.

4.1. Evaluation Criteria. To quantitatively describe the performance of the model, the indicators of mean absolute percentage error (MAPE), mean-squared error (MSE), and *R*-squared (*R*²) are used to measure the performance of the model. MAPE reflects the accuracy of the model, MSE reflects the deviation between simulation data and modeling results, and *R*² represents the matching degree between the modeling results and simulation data.

$$\text{MAPE} = \frac{1}{n} \sum_{i=1}^n \frac{|z_i - y_i|}{y_i} \times 100\% \quad (11)$$

$$\text{MSE} = \frac{1}{n} \sum_{i=1}^n (z_i - y_i)^2 \quad (12)$$

$$R^2 = 1 - \frac{(\sum_{i=1}^n (z_i - y_i)^2)/n}{(\sum_{i=1}^n (y_i - \bar{y})^2)/n} = 1 - \frac{\text{MSE}(z, y)}{\text{Var}(y)} \quad (13)$$

where *n* is the number of samples, *z*_{*i*} is the modeling results of the model, and *y*_{*i*} is the simulation value.

Table 3. Sort Order by Variables' Importance

sort	variables	importance coefficient
1	<i>x</i> -coordinate	1.000 × 10 ⁰
2	O ₂ concentration	1.569 × 10 ^{−1}
3	CO concentration	5.321 × 10 ^{−2}
4	<i>z</i> -coordinate	4.752 × 10 ^{−2}
5	<i>y</i> -coordinate	4.067 × 10 ^{−2}
6	pressure	4.057 × 10 ^{−2}
7	temperature	2.675 × 10 ^{−2}
8	the total energy	1.482 × 10 ^{−2}
9	H ₂ O concentration	1.252 × 10 ^{−2}
10	volatile concentration	6.993 × 10 ^{−3}
11	CO ₂ concentration	4.583e × 10 ^{−4}
12	<i>z</i> -velocity	3.522 × 10 ^{−4}
13	radial velocity	1.325 × 10 ^{−4}
14	relative velocity angle	8.658 × 10 ^{−5}
15	<i>x</i> -velocity	7.051 × 10 ^{−5}
16	<i>y</i> -velocity	2.701 × 10 ^{−5}
17	total pressure	2.188 × 10 ^{−5}
18	N ₂ concentration	1.357 × 10 ^{−5}
19	radiation temperature	1.238 × 10 ^{−5}
20	<i>x</i> -vorticity	1.697 × 10 ^{−7}
21	<i>y</i> -vorticity	5.881 × 10 ^{−13}
22	<i>z</i> -vorticity	0
23	density	0

Table 4. Modeling Data Information

variables	range	unit
temperature	[330.52, 1852.86]	K
<i>x</i> -coordinates	[−6.03, 3.19]	m
<i>y</i> -coordinates	[−2, 2]	m
<i>z</i> -coordinates	[0, 26.38]	m
CO concentration	[0, 0.0014]	kmol/m ³
O ₂ concentration	[1.60 × 10 ^{−11} , 0.0069]	kmol/m ³
H ₂ O concentration	[0, 0.00117]	kmol/m ³
volatile concentration	[10, 65]	mol/m ³
SO ₂ concentration	[0, 1.87 × 10 ^{−5}]	kmol/m ³
total energy	[−2 336 317, 448 157]	J/kg
pressure	[−553.73, 2980.15]	Pa

4.2. Result Analysis. **4.2.1. Distribution of the Prediction Error.** To demonstrate the feasibility of using the LDBN model for correlation analysis of SO₂ distribution with other POCs, the absolute error between the simulation data and the modeling data of LDBN is displayed in Figure 6.

A comparison of the simulation data with the modeling data shows that the combustion model based on CFD can reasonably simulate the combustion process of the furnace.

Thus, the simulation data obtained by CFD simulations can be used to correlate SO₂ distribution with other POCs.

In Figure 6a,b, most areas of the XOZ section and XOY section are blue (error less than 3.7 × 10^{−7} kmol/m³). However, due to the chemical reaction in the middle bottom area during the combustion of the furnace, a few areas at the bottom of the furnace are green (error less than 9.6 × 10^{−7} kmol/m³) in the XOZ section.

It can be seen from Figure 6 that most of the error distribution areas are blue, which indicates that LDBN can mine deep data information, so it is feasible to use LDBN to reveal the correlation between SO₂ distribution and combustion products.

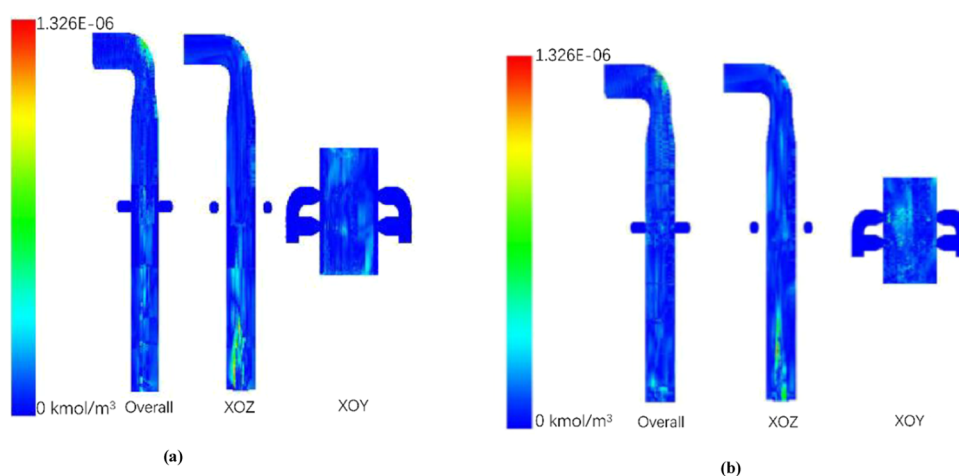


Figure 6. Distribution of the error of different swing angles: (a) angle equal to 30° and (b) angle equal to 55°.

Table 5. Influence of Feature Selection on Modeling Results

data set	evaluation criteria	30°			55°		
		Lasso	Pearson	none	Lasso	Pearson	none
Data 1	MAPE	1.600^{at}	3.419	1.610	1.320^{at}	8.112	1.450
	MSE	4.84 × 10^{-15at}	2.01 × 10 ⁻¹⁴	5.41 × 10 ⁻¹⁵	8.55 × 10^{-15at}	5.24 × 10 ⁻¹³	1.19 × 10 ⁻¹⁴
	R ²	0.999^{at}	0.997	0.998	0.999^{at}	0.940	0.998
	time	6271.420^{at}	6447.027	6685.680	5318.900^{at}	5489.073	5771.160
Data 2	MAPE	2.940	4.671	2.640^{at}	1.490^{at}	4.952	1.590
	MSE	1.28 × 10 ⁻¹⁴	3.67 × 10 ⁻¹⁴	1.19 × 10^{-14at}	6.31 × 10^{-15at}	1.08 × 10 ⁻¹³	7.60 × 10 ⁻¹⁵
	R ²	0.998	0.995	0.999^{at}	0.999^{at}	0.915	0.998
	time	6097.690^{at}	6437.314	7000.120	6324.860^{at}	6480.189	6685.620
Data 3	MAPE	3.050	4.812	3.020^{at}	1.720^{at}	2.200	1.819
	MSE	2.65 × 10 ⁻¹⁴	4.35 × 10 ⁻¹⁴	2.55 × 10^{-14at}	9.27 × 10^{-15at}	1.47 × 10 ⁻¹⁴	9.23 × 10 ⁻¹⁴
	R ²	0.996	0.994	0.997^{at}	0.998^{at}	0.982	0.997
	time	6254.540^{at}	6467.775	6270.610	6089.450^{at}	6474.579	6313.940
Data 4	MAPE	5.530^{at}	6.396	6.810	4.470	2.797^{at}	4.710
	MSE	3.09 × 10 ⁻¹⁴	1.88 × 10 ⁻¹³	2.76 × 10^{-14at}	2.36 × 10 ⁻¹⁴	4.91 × 10 ⁻¹⁴	1.74 × 10^{-14at}
	R ²	0.997	0.972	0.998^{at}	0.997	0.975	0.998^{at}
	time	6578.880^{at}	6612.006	6972.400	6088.880^{at}	6477.989	6839.440
Data 5	MAPE	6.610	7.020	6.530^{at}	3.960	1.456^{at}	5.380
	MSE	3.42 × 10 ⁻¹⁴	2.47 × 10 ⁻¹³	2.61 × 10^{-14at}	1.66 × 10 ⁻¹⁴	1.57 × 10^{-14at}	1.78 × 10 ⁻¹⁴
	R ²	0.996	0.968	0.997^{at}	0.997^{at}	0.993	0.996
	time	6045.890^{at}	6406.274	6693.440	6327.040^{at}	6482.084	6676.350
Data 6	MAPE	3.820	22.026	3.090^{at}	2.400	2.518	1.680^{at}
	MSE	2.21 × 10 ⁻¹⁴	1.14 × 10 ⁻¹³	1.64 × 10^{-14at}	1.24 × 10 ⁻¹⁴	1.55 × 10 ⁻¹⁴	9.21 × 10^{-15at}
	R ²	0.996	0.982	0.997^{at}	0.997	0.995	0.998^{at}
	time	5911.370^{at}	6406.274	6947.740	6119.520^{at}	6486.819	6981.860
Data 7	MAPE	2.600	4.452	2.340^{at}	1.380	1.153	0.960^{at}
	MSE	1.06 × 10^{-14at}	3.79 × 10 ⁻¹⁴	1.11 × 10 ⁻¹⁴	5.69 × 10 ⁻¹⁵	4.67 × 10 ⁻¹⁵	3.98 × 10^{-15at}
	R ²	0.999^{at}	0.994	0.998	0.999	0.999	0.999
	time	5504.840^{at}	5624.638	5697.030	5191.720^{at}	5425.850	5683.490
Data 8	MAPE	2.280^{at}	4.722	2.430	1.150	2.100	1.140^{at}
	MSE	7.41 × 10^{-15at}	6.00 × 10 ⁻¹⁴	8.89 × 10 ⁻¹⁵	4.75 × 10^{-15at}	1.64 × 10 ⁻¹⁴	5.87 × 10 ⁻¹⁵
	R ²	0.999^{at}	0.995	0.998	0.999^{at}	0.998	0.996
	time	5412.640^{at}	5478.110	5656.880	5491.670	5420.303^{at}	5629.590

^{at}The evaluation index of the results in bold is significantly better than other algorithms.

4.2.2. Influence of Feature Selection on Modeling Accuracy. To verify the influence of the Lasso method for feature selection on modeling efficiency, three groups of comparative experiments are conducted on the DBN model (Table 5). The first group takes the input of 10 variables after Lasso feature selection, the second group takes the input of 10

variables after feature selection by Pearson correlation, and the third group takes the input of 23 variables without feature selection. The results show that when the swing angle is 30°, the R² values of the eight data sets before and after using Lasso feature selection are similar, but the modeling time after Lasso feature selection is reduced by 7.2% on average. The MAPE and

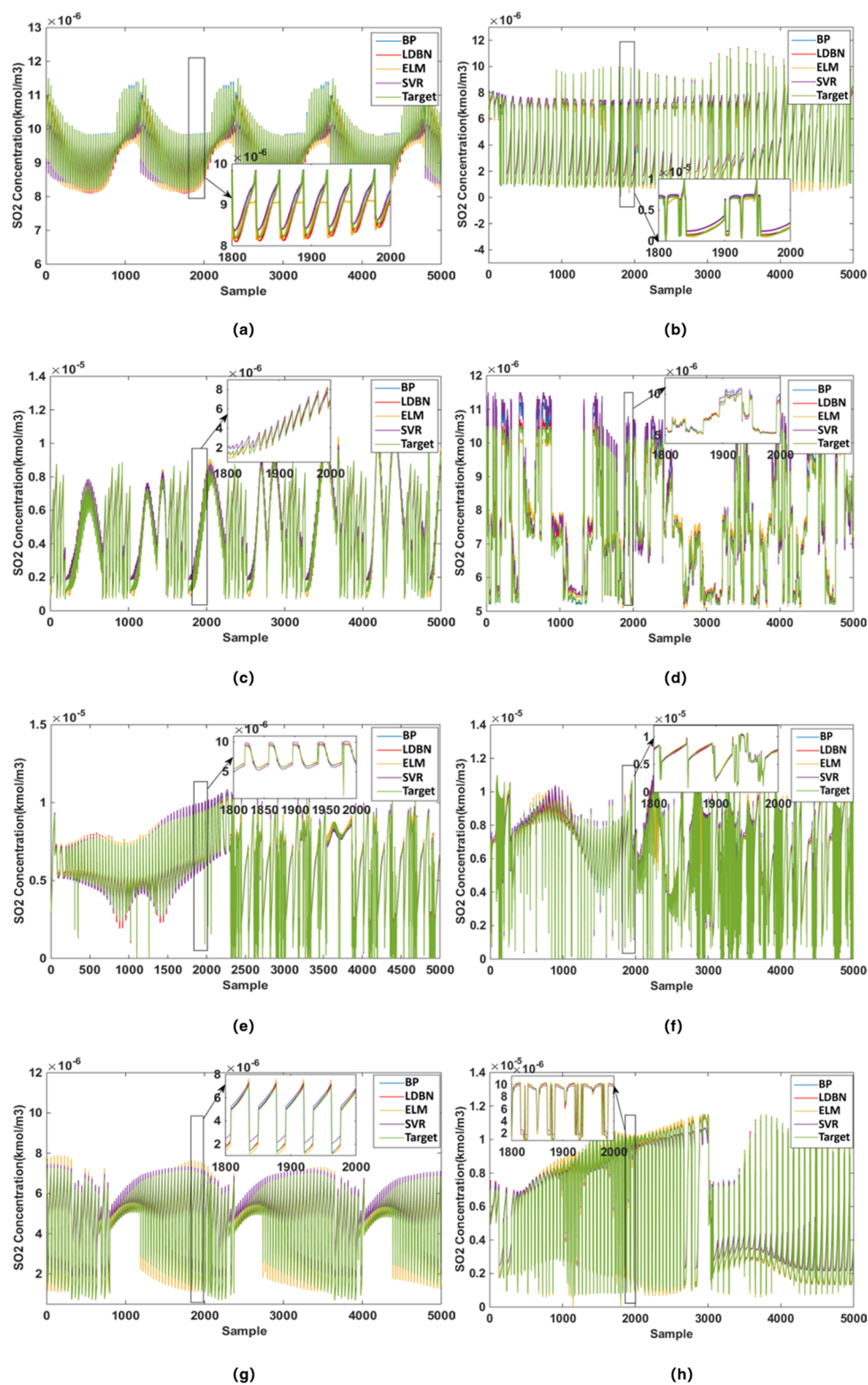


Figure 7. Results of different algorithms under a swing angle of 30° : (a) Data 1, (b) Data 2, (c) Data 3, (d) Data 4, (e) Data 5, (f) Data 6, (g) Data 7, and (h) Data 8.

MSE of Data 1 after Lasso feature selection are improved by 0.6 and 10.54%, respectively; the MAPE and MSE of Data 8 are also improved by 6.17 and 16.64%, respectively. When the swing angle is 55° , the time of Data 1 is reduced by about 7.8%, and the MAPE and MSE are improved by 6.2 and 28.15%, respectively, after Lasso feature selection. As for Data 2, there is no significant change in accuracy before and after Lasso feature selection, but

the modeling time is reduced by about 361 s. Therefore, the efficiency of the model is improved after feature selection. Compared with using the Pearson correlation method, the model built using the lasso method for feature selection has higher accuracy. On Data 2 of 30° swing angle, the MAPE, MSE, and R^2 of the Lasso are respectively improved by 43.46, 65.12, and 0.2%. On Data 3 of 55° swing angle, the MAPE, MSE, and

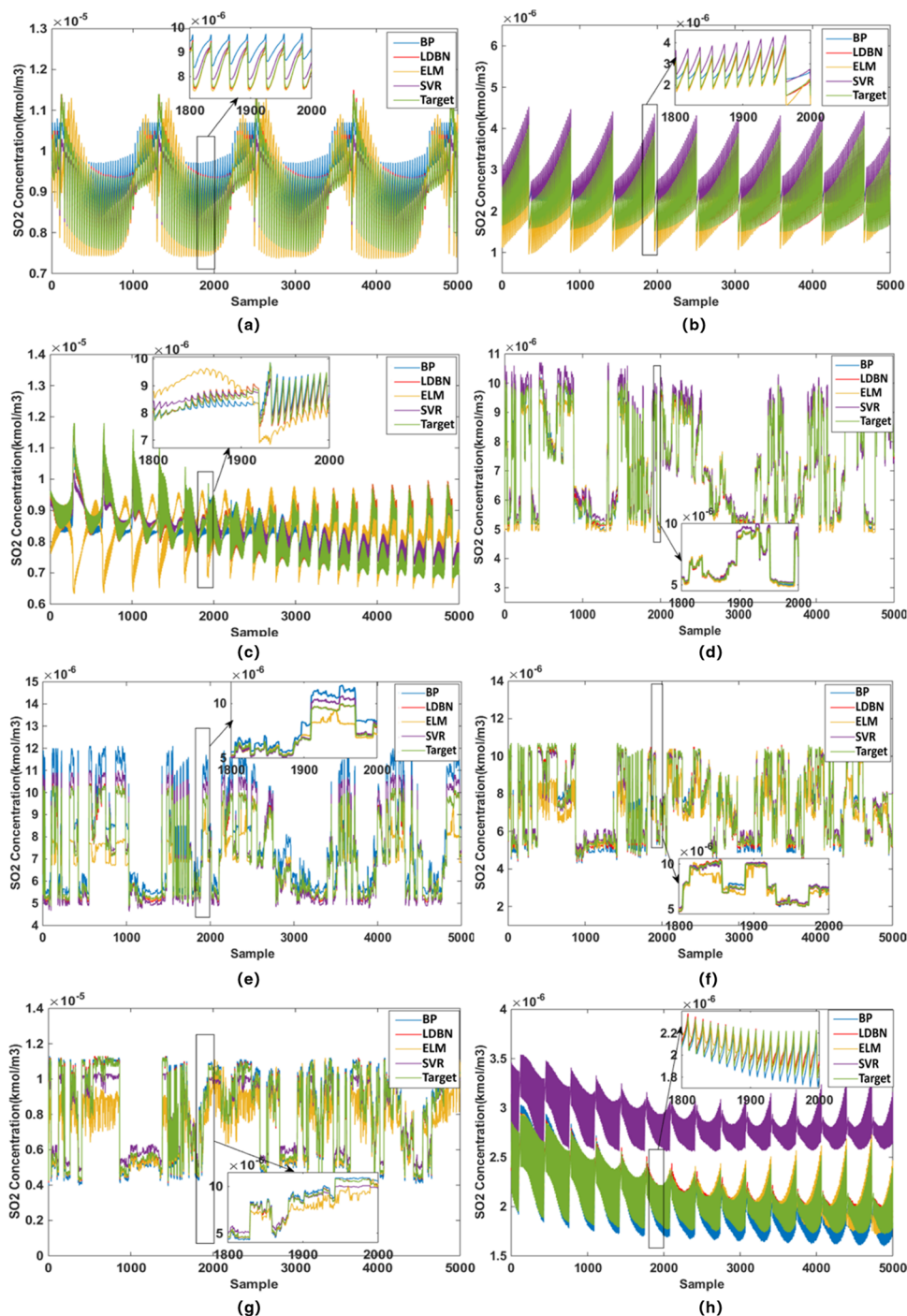


Figure 8. Results of different algorithms under a swing angle of 55° : (a) Data 1, (b) Data 2, (c) Data 3, (d) Data 4, (e) Data 5, (f) Data 6, (g) Data 7, and (h) Data 8.

R^2 of the Lasso are respectively improved by 83.9, 36.93, and 1.6%. Since the Pearson correlation method can only select linearly correlated features, some nonlinearly correlated features are not screened out. Therefore, the Lasso method is more suitable for selecting feature variables than the Pearson correlation method.

4.2.3. Influence of Different Algorithms on Modeling Accuracy. To more intuitively reflect the accuracy and generalization ability of the SO_2 distribution model based on LDBN, the results of our proposed model are compared with those of the BP neural network, extreme learning machine

(ELM), and support vector regression (SVR). Figures 7 and 8 respectively show the results of the four different algorithms on the eight data sets under the swing angles of 30° and 55° . It can be seen from the figures that the four algorithms achieve good correlation analysis results for SO_2 in the furnace.

In comparison, the variation trend of the results obtained by LDBN is closer to the simulation data trend, indicating that the model based on LDBN has a better fitting ability. It can be seen from the box diagram in Figure 9 that compared with other algorithms, the error of LDBN is closer to error line 0 and there are relatively fewer outliers. In contrast, the excessive error of

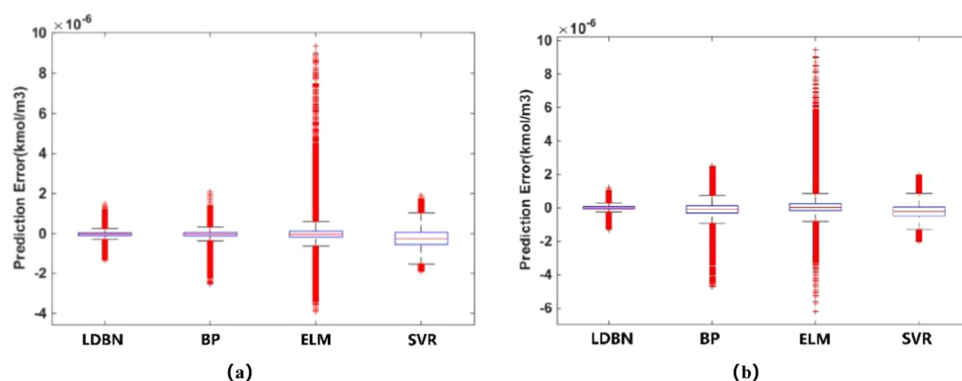


Figure 9. Boxplot of the error of different algorithms on different data sets under the two swing angles of (a) 30° and (b) 55°.

Table 6. Comparison of Performance of Different Models under a Swing Angle of 30°

data set	evaluation criteria	LDBN	BP	ELM	SVR
Data 1	MAPE	1.600 ^a	1.770	6.030	10.210
	MSE	4.84×10^{-15a}	7.26×10^{-15}	8.45×10^{-14}	1.47×10^{-13}
	R ²	0.999 ^a	0.998	0.993	0.986
Data 2	MAPE	2.940 ^a	4.300	11.720	20.740
	MSE	1.28×10^{-14a}	2.98×10^{-14}	2.35×10^{-13}	2.51×10^{-13}
	R ²	0.998 ^a	0.996	0.969	0.962
Data 3	MAPE	3.050 ^a	3.690	7.560	18.470
	MSE	2.65×10^{-14a}	4.26×10^{-14}	3.08×10^{-13}	3.67×10^{-13}
	R ²	0.997 ^a	0.994	0.958	0.949
Data 4	MAPE	5.530 ^a	7.120	14.880	80.860
	MSE	3.09×10^{-14a}	4.50×10^{-14}	1.07×10^{-13}	3.19×10^{-13}
	R ²	0.997 ^a	0.996	0.990	0.968
Data 5	MAPE	6.610 ^a	8.390	14.870	56.350
	MSE	3.42×10^{-14a}	4.12×10^{-14}	1.02×10^{-13}	1.47×10^{-13}
	R ²	0.996 ^a	0.995	0.987	0.980
Data 6	MAPE	3.802 ^a	4.540	7.110	6.340
	MSE	2.21×10^{-14a}	3.91×10^{-14}	8.07×10^{-14}	7.31×10^{-14}
	R ²	0.997 ^a	0.994	0.987	0.988
Data 7	MAPE	2.600 ^a	4.310	10.940	20.290
	MSE	1.06×10^{-14a}	3.14×10^{-14}	2.50×10^{-13}	3.16×10^{-13}
	R ²	0.999 ^a	0.996	0.968	0.949
Data 8	MAPE	2.280 ^a	2.620	5.650	22.540
	MSE	7.40×10^{-15a}	1.15×10^{-14}	7.24×10^{-14}	4.90×10^{-13}
	R ²	0.999 ^a	0.998	0.996	0.960

^aThe evaluation index of the results is significantly better than other algorithms.

ELM may be due to the fact that as a shallow network, the ability to map to high-dimensional space is insufficient and the correlation between variables cannot be explored more deeply. To further analyze the fitting effect of LDBN and the other three algorithms, the values of the error evaluation indicators on the eight data sets under the two swing angles are listed in Tables 6 and 7.

In Table 6, the mean values of MAPE of LDBN, BP, ELM, and SVR algorithms are 3.55, 4.59, 9.85, and 29.48%; the average values of MSE are 1.87×10^{-14} , 3.10×10^{-14} , 1.55×10^{-13} , and 1.55×10^{-13} kmol/m³; and the average values of R² reach 0.998, 0.996, 0.981, and 0.968, respectively. These results indicate that the model based on LDBN has better fitting effect.

Meanwhile, as shown in Table 7, compared with the ELM algorithm, the MAPE and MSE of the LDBN algorithm on Data 1 are respectively improved by 76.4 and 34.6%, and the difference of R² is 0.0274. LDBN can dig out the deep feature information contained in the data, so the values of MAPE and MSE are much better. On Data 2, the MAPE, MSE, and R² of the

LDBN algorithm are respectively improved by 81.9, 59.9, and 4.3%. On Data 3, the MAPE and R² of the LDBN algorithm are improved by 10.67% and 0.0648, respectively, while the MSE is improved by about 53%. In summary, the fitting ability of LDBN is improved under the swing angles of 30 and 55°, and all of the error evaluation indicators are optimal. These results indicate that LDBN achieves a better effect in the correlation analysis of SO₂ distribution in the furnace.

The relationship between SO₂ distribution and other combustion products in the process of coal combustion is very complicated, but LDBN can still capture the relevant regulations through data. It can fully learn and dig into the correlation between SO₂ distribution regulations and other combustion products.

4.3. Sensitivity Analysis. To reveal the influence of various parameters of SO₂ distribution in the furnace, a sensitivity analysis was conducted. In the sensitivity analysis, the parameters and other conditions of the model are kept the same, and only the influence of the changes of each input

Table 7. Comparison of Performance of Different Models under a Swing Angle of 55°

data set	evaluation criteria	LDBN	BP	ELM	SVR
Data 1	MAPE	1.320 ^{at}	9.850	5.590	8.120
	MSE	8.55 × 10 ^{-15a}	4.35 × 10 ⁻¹³	1.77 × 10 ⁻¹³	1.20 × 10 ⁻¹³
	R ²	0.999 ^{at}	0.934	0.971	0.975
Data 2	MAPE	1.490 ^{at}	17.350	8.220	11.290
	MSE	6.31 × 10 ^{-15a}	7.43 × 10 ⁻¹³	2.13 × 10 ⁻¹³	1.78 × 10 ⁻¹³
	R ²	0.999 ^{at}	0.720	0.956	0.957
Data 3	MAPE	1.720 ^{at}	22.870	12.390	16.350
	MSE	9.27 × 10 ^{-15a}	2.24 × 10 ⁻¹³	2.67 × 10 ⁻¹³	3.27 × 10 ⁻¹³
	R ²	0.998 ^{at}	0.946	0.933	0.910
Data 4	MAPE	4.470 ^{at}	4.920	13.970	56.970
	MSE	2.36 × 10 ^{-14a}	2.58 × 10 ⁻¹⁴	9.44 × 10 ⁻¹⁴	2.17 × 10 ⁻¹³
	R ²	0.997 ^{at}	0.997	0.988	0.971
Data 5	MAPE	3.960 ^{at}	28.680	29.200	34.900
	MSE	1.66 × 10 ^{-14a}	4.63 × 10 ⁻¹³	3.28 × 10 ⁻¹³	1.77 × 10 ⁻¹³
	R ²	0.997 ^{at}	0.939	0.947	0.975
Data 6	MAPE	2.400 ^{at}	8.170	12.050	3.630
	MSE	1.24 × 10 ^{-14a}	6.44 × 10 ⁻¹⁴	4.51 × 10 ⁻¹³	3.93 × 10 ⁻¹⁴
	R ²	0.998 ^{at}	0.988	0.904	0.992
Data 7	MAPE	1.380 ^{at}	3.540	8.530	10.560
	MSE	5.69 × 10 ^{-15a}	4.69 × 10 ⁻¹⁴	5.49 × 10 ⁻¹³	2.08 × 10 ⁻¹³
	R ²	0.999 ^{at}	0.995	0.928	0.966
Data 8	MAPE	1.150 ^{at}	4.000	5.250	13.190
	MSE	4.75 × 10 ^{-15a}	8.80 × 10 ⁻¹⁴	3.11 × 10 ⁻¹³	4.12 × 10 ⁻¹³
	R ²	0.999 ^{at}	0.995	0.981	0.968

^aThe evaluation index of the results is significantly better than other algorithms.

variable on the SO₂ distribution is studied. Therefore, when analyzing each variable, each input variable is replaced by the mean value sequence, and a SO₂ distribution model is established to obtain MAPE. The results are shown in Figure 10. The first column shows the MAPE of the original model

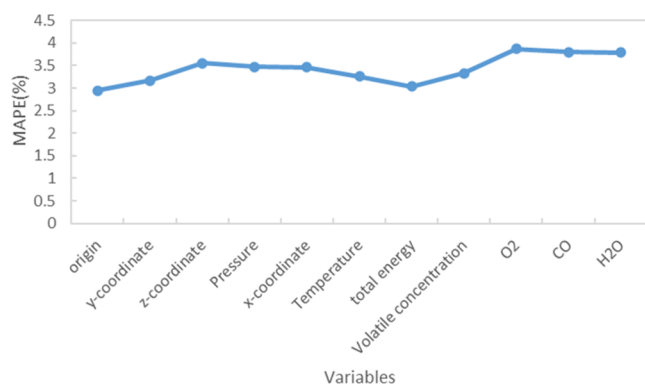


Figure 10. Sensitivity analysis results.

without changing the input variables, and the 2nd–11th columns show the MAPE of the model established after each input variable is replaced by the mean. It can be seen from the figure that when the mean value is used instead of O₂, the error of the training set and the test set increases the most and the MAPE reaches 3.8671, which is a 23.97% increase in MAPE compared with the original model origin. CO also has a great influence on SO₂ distribution, with a 23.64% increase in MAPE. In contrast, the total energy has the least impact on SO₂ distribution, and MAPE is increased by 2.97%. The above results show that there is a strong correlation between the concentration of O₂ and the concentration of CO in SO₂ distribution.

4.4. Discussion of Results. According to the analysis of the results in the previous section, the following observations can be made:

- (1) Data preprocessing can improve the accuracy of the model. Because there is no combustion reaction or insufficient combustion in some areas of the furnace, there are some zero values and minimum values in the simulation data of CFD, which will affect the accuracy of the model. Therefore, the accuracy of the model is improved by data preprocessing.
- (2) Feature selection can improve the modeling accuracy. The characteristics of uneven quality, high dimension, and little correlation of the data affect the accuracy of the model. Thus, it is necessary to select features. In this study, the Lasso method is used to select features from the simulation data, and the results show that feature selection can effectively improve the modeling accuracy and reduce the modeling time.
- (3) LDBN is suitable for modeling SO₂ distribution in furnaces. The comparison of the results of LDBN to those of BP, ELM, and SVR shows that LDBN achieves higher accuracy and better fitting ability in the correlation model of SO₂ distribution in the furnace. The sensitivity analysis is performed to determine the correlation between the input variables for SO₂ distribution, and the analysis is conducted by changing the values of the input variables. The results show that O₂ concentration has the highest influence on SO₂ distribution, followed by CO concentration. The total energy has the least influence on SO₂ distribution. The slight changes in O₂ concentration, CO concentration, and total energy lead to improvements in MAPE by about 23.97, 23.64, and 2.97%, respectively.

5. CONCLUSIONS

A model based on LDBN is proposed in this paper, which uses the CFD simulation data of a 30 MW furnace to analyze the relationship between SO₂ distribution and other POCs in the furnace. First, the CFD numerical simulation is conducted on the test bench under different burner swing angles and the obtained simulation data is taken as the experimental data. Then, the Lasso method is used to select ten variables with a high correlation with SO₂ distribution as the input of the DBN model, and a correlation model of SO₂ distribution in the furnace based on LDBN is established. By comparing the analysis results of LDBN to those of BP, ELM, and SVR, it is verified that the correlation model established in this paper can accurately predict the SO₂ distribution in the furnace with better prediction accuracy and generalization ability. It is proved that there is a strong correlation between SO₂ distribution, O₂ concentration, and CO concentration. This makes it convenient for operators to understand the combustion situation and provide theoretical support for the subsequent control and emission reduction of SO₂ and other gases.

AUTHOR INFORMATION

Corresponding Author

Zhenhao Tang – School of Automation Engineering, Northeast Electric Power University, Jilin 132012, China; orcid.org/0000-0002-4650-6870; Email: tangzhenhao@neepu.edu.cn

Authors

Hongrui Dong – School of Automation Engineering, Northeast Electric Power University, Jilin 132012, China
Chong Zhang – School of Automation Engineering, Northeast Electric Power University, Jilin 132012, China
Shengxian Cao – School of Automation Engineering, Northeast Electric Power University, Jilin 132012, China
Tinghui Ouyang – Artificial Intelligence Research Center (AIRC), National Institute of Advanced Industrial Science and Technology (AIST), Tokyo 135-0064, Japan

Complete contact information is available at:

<https://pubs.acs.org/10.1021/acsomega.2c03468>

Notes

The authors declare no competing financial interest.

ACKNOWLEDGMENTS

This project was supported by the Jilin Science and Technology Project under Grant 20200401085GX.

REFERENCES

- (1) Xiong, X.; Liu, X.; Tan, H.; Deng, S. Investigation on high temperature corrosion of water-cooled wall tubes at a 300 MW boiler. *Energy Inst.* **2020**, *93*, 377–386.
- (2) Jin, Q.; Dai, G.; Wang, Y.; Wang, Z.; Shan, Z.; Wang, X.; Zhang, L.; Tan, H. Z.; Mikulčić, H. High-temperature corrosion of water-wall tubes in oxy-combustion atmosphere. *J. Energy Inst.* **2020**, *93*, 1305–1312.
- (3) Belošević, S.; Ivan, T.; Nenad, C.; Aleksandar, M.; Dragan, T. Numerical study of pulverized coal-fired utility boiler over a wide range of operating conditions for in-furnace SO₂/NO_x reduction. *Appl. Therm. Eng.* **2016**, *94*, 657–669.
- (4) Zhang, Z. L.; Zeng, Q. D. Numerical simulation and experimental analysis on nitrogen and sulfur oxides emissions during the co-combustion of Longyan anthracite and sawmill sludge. *Fuel* **2019**, *254*, 115611.

- (5) Azeez, W. S.; Hasini, H.; Yusoff, Z. CFD investigation of the effect of tilt angles to flow and combustion in a 120 MW gas-fired full scale industrial boiler. *Int. J. Sci. Technol. Res.* **2015**, *4*, 164–170.
- (6) Adamczyk, W. P.; Isaac, B.; Parra-Alvarez, J.; Smith, S. T.; Harris, D.; Thornock, J.; Zhou, M. M.; Smith, P. J.; Zmuda, R. Application of LES-CFD for predicting pulverized-coal working conditions after installation of NO_x control system. *Energy* **2018**, *160*, 693–709.
- (7) Madejski, P. Numerical study of a large-scale pulverized coal-fired boiler operation using CFD modeling based on the probability density function method. *Appl. Therm. Eng.* **2018**, *145*, 352–363.
- (8) Tian, Z. F.; Witt, P. J.; Schwarz, M. P.; Yang, W. Numerical modeling of victorian brown coal combustion in a tangentially fired furnace. *Energy Fuels* **2010**, *24*, 4971–4979.
- (9) Modlinski, N.; Hardy, T. Development of high-temperature corrosion risk monitoring system in pulverized coal boilers based on reducing conditions identification and CFD simulations. *Appl. Energy* **2017**, *204*, 1124–1137.
- (10) Ji, J.; Cheng, L.; Wei, Y.; Wang, J.; Wang, Q. Predictions of NO_x/N₂O emissions from an ultra-supercritical CFB boiler using a 2-D comprehensive CFD combustion model. *Particuology* **2020**, *49*, 77–87.
- (11) Choi, C. R.; Chang, N. K. Numerical Investigation on the Flow, Combustion and NO_x Emission Characteristics in A 500 MW, Tangentially Fired Pulverized-Coal Boiler. *Fuel* **2009**, *88*, 1720–1731.
- (12) Dal Secco, S.; Juan, O.; Louis-Louis, M.; Lucas, J. Y.; Plion, P.; Porcheron, L. Using a genetic algorithm and CFD to identify low NO_x configurations in an industrial boiler. *Fuel* **2015**, *158*, 672–683.
- (13) Du, Y. B.; Wang, C. A.; Lv, Q.; Li, D. B.; Liu, H. CFD investigation on combustion and NO_x emission characteristics in a 600 MW wall-fired boiler under high temperature and strong reducing atmosphere. *Appl. Therm. Eng.* **2017**, *126*, 407–418.
- (14) Tan, P.; Tian, D.; Fang, Q.; Ma, L.; Zhang, C.; Chen, G.; Zhong, L.; Zhang, H. Effects of burner tilt angle on the combustion and NO_x emission characteristics of a 700 MWe deep-air-staged tangentially pulverized-coal-fired boiler. *Fuel* **2017**, *196*, 314–324.
- (15) Srinivas, S. M.; Keerthi, N. P.; Sakshi, N.; Kishalay, M. Evolutionary neural architecture search for surrogate models to enable optimization of industrial continuous crystallization process. *Powder Technol.* **2022**, *405*, No. 117527.
- (16) Inapakurthi, R. K.; Kishalay, M. Optimal surrogate building using SVR for an industrial grinding process. *Mater. Manuf. Processes* **2022**, *37*, 1701–1707.
- (17) Tang, Z. H.; Wang, S. K.; Chai, X. Y.; Cao, S. X.; Ouyang, T. H.; Li, Y. Auto-encoder-extreme learning machine model for boiler NO_x emission concentration prediction. *Energy* **2022**, *256*, No. 124552.
- (18) Mogilicharla, A.; Prateek, M.; Saptarshi, M.; Kishalay, M. Kriging surrogate based multi-objective optimization of bulk vinyl acetate polymerization with branching. *Mater. Manuf. Processes* **2015**, *30*, 394–402.
- (19) Lv, Y.; Hong, F.; Yang, T.; Fang, F.; Liu, J. A dynamic model for the bed temperature prediction of circulating fluidized bed boilers based on least squares support vector machine with real operational data. *Energy* **2017**, *124*, 284–294.
- (20) Yang, G.; Wang, Y.; Li, X. Prediction of the NO_x emissions from thermal power plant using long-short term memory neural network. *Energy* **2020**, *192*, 116597.
- (21) Tan, P.; He, B.; Zhang, C.; Rao, D. B.; Li, S. N.; Fang, Q. Y.; Chen, G. Dynamic modeling of NO_x emission in a 660 MW coal-fired boiler with long short-term memory. *Energy* **2019**, *176*, 429–436.
- (22) Tang, Z. H.; Zhang, Z. J. The multi-objective optimization of combustion system operations based on deep data-driven models. *Energy* **2019**, *182*, 37–47.
- (23) Wang, F.; Ma, S.; He, W.; Li, Y. D.; Qin, Z. G.; Zhang, J. J. A hybrid model integrating improved flower pollination algorithm-based feature selection and improved random forest for NO_x emission estimation of coal-fired power plants. *Measurement* **2018**, *125*, 303–312.
- (24) Krzywanski, J.; Czakiert, T.; Blaszcuk, A.; Rajczyk, R.; Muskala, W.; Nowak, W. A generalized model of SO₂ emissions from large and small-scale CFB boilers by artificial neural network approach part 1.

The mathematical model of SO₂ emissions in air-firing, oxygen-enriched and oxy-combustion CFB conditions. *Fuel Process. Technol.* **2015**, *137*, 66–74.

(25) Krzywanski, J.; Czakiert, T.; Blaszcuk, A.; Rajczyk, R.; Muskala, W.; Nowak, W. A generalized model of SO₂ emissions from large and small-scale CFB boilers by artificial neural network approach part 2. SO₂ emissions from large- and pilot-scale CFB boilers in O₂ /N₂, O₂ /CO₂ and O₂ /RFG combustion atmospheres. *Fuel Process. Technol.* **2015**, *139*, 73–85.

(26) Wen, J. M.; Yan, J. H.; Zhang, D. P.; Chi, Y.; et al. SO₂ emission characteristics and BP neural networks prediction in MSW/coal co-fired fluidized beds. *J. Therm. Sci.* **2006**, *15*, 281–288.

(27) Yu, H. Y.; Gao, M. M.; Zhang, H. F.; Chen, Y. Dynamic modeling for SO₂-NO_x emission concentration of circulating fluidized bed units based on quantum genetic algorithm - extreme learning machine. *J. Cleaner Prod.* **2021**, *324*, 129170.

(28) Ran, P.; Wang, Y.; Liu, P.; Li, Z. A fuzzy association rule mining based approach to identifying SO₂ emission concentration patterns of coal-fired boilers. *Chem. Eng. Trans.* **2016**, *52*, 631–636.

(29) Pai, T. Y.; Lo, H. M.; Wan, T. J.; Chen, L.; Hung, P. S.; Lo, H. H.; Lai, W. J.; Lee, H. Y. Predicting air pollutant emissions from a medical incinerator using grey model and neural network. *Appl. Math. Model.* **2015**, *39*, 1513–1525.

(30) Hinton, G. E.; Osindero, S.; Teh, Y. W. A fast learning algorithm for deep belief nets. *Neurocomputing* **2006**, *18*, 1527–1554.

(31) Kim, S.; Park, B.; Song, B. S.; Yang, S. Deep belief network based statistical feature learning for fingerprint liveness detection. *Pattern Recognit. Lett.* **2016**, *77*, 58–65.

(32) Zhao, Z.; Jiao, L.; Zhao, J.; Gu, J.; Jin, Z. Discriminant deep belief network for high-resolution SAR image classification. *Pattern Recognit.* **2017**, *61*, 686–701.

(33) Tibshirani, R. Regression shrinkage and selection via the Lasso. *J. R. Stat. Soc., Ser. B* **1996**, *58*, 267–288.

(34) Mohr, M.; Klaniar, M.; Schloen, T.; Samec, N.; Kokalj, F. Numerical analysis of a non-steady state phenomenon during the ignition process in a condensing boiler. *Energy* **2018**, *158*, 623–631.

(35) Wang, C. Q.; Ma, J. C.; Zhao, H. B.; Zheng, Y. Sulfur evolution in chemical looping combustion of coal. *J. Eng. Thermophys.* **2020**, *41*, 229–237.